applied sciences

MDPI

Article

One-Dimensional Optimization Design of Supercritical Carbon Dioxide Radial Inflow Turbine and Performance Analysis under Off-Design Conditions

Zhiting Tong [1,2], Zedong Song [1,2], Chao Zhang [1,2,*], Hao Xing [1,2] and Yuxuan Sun [3]

1 Tianjin Key Laboratory for Advanced Mechatronic System Design and Intelligent Control, School of Mechanical Engineering, Tianjin University of Technology, Tianjin 300384, China; tongzhiting1215@163.com (Z.T.); songzedong_525@163.com (Z.S.); xinghao19940403@163.com (H.X.)
2 National Demonstration Center for Experimental Mechanical and Electrical Engineering Education (Tianjin University of Technology), Tianjin 300384, China
3 Institute of Engineering Thermophysics, Chinese Academy of Sciences, Beijing 100190, China; sunyuxuan@iet.cn
* Correspondence: czhangxj@email.tjut.edu.cn

Abstract: In the present study, the one-dimensional optimization design and the performance analysis based on a three-dimensional model were performed for a 2.1 MW supercritical carbon dioxide radial inflow turbine. Firstly, an in-house code was developed with MATLAB language for one-dimensional optimization design to maximize the total-to-static efficiency. Then, the three-dimensional radial inflow turbine model was constructed based on the one-dimensional optimization design result. Finally, the flow field and the aerodynamic performance were studied using the commercial software NUMECA. It is shown that the total-to-static efficiency obtained from three-dimensional simulation under the nominal design condition is 85.77%, with a relative deviation of 0.55%, as compared with that from the one-dimensional optimization design. Furthermore, the static temperature and pressure from the turbine inlet to the outlet drop uniformly, and there is no obvious flow separation under the nominal design condition. The values of total-to-static efficiency are always higher than 75% at the 80–110% relative rotating speed and the expansion ratio of 1.75–4.48, which also demonstrates good performance under the off-design working conditions.

Keywords: supercritical carbon dioxide; radial inflow turbine; one-dimensional optimization design; off-design performance; numerical simulation

check for updates

Citation: Tong, Z.; Song, Z.; Zhang, C.; Xing, H.; Sun, Y. One-Dimensional Optimization Design of Supercritical Carbon Dioxide Radial Inflow Turbine and Performance Analysis under Off-Design Conditions. *Appl. Sci.* **2022**, *12*, 3882. https://doi.org/10.3390/app12083882

Academic Editor: Satoru Okamoto

Received: 23 March 2022
Accepted: 10 April 2022
Published: 12 April 2022

Publisher's Note: MDPI stays neutral with regard to jurisdictional claims in published maps and institutional affiliations.

Copyright: © 2022 by the authors. Licensee MDPI, Basel, Switzerland. This article is an open access article distributed under the terms and conditions of the Creative Commons Attribution (CC BY) license (https://creativecommons.org/licenses/by/4.0/).

1. Introduction

The Brayton cycle with supercritical carbon dioxide (s-CO_2) as a working fluid has raised universal attention in the last few decades [1]. The s-CO_2 Brayton cycle exhibits a few advantages compared with the Brayton cycle with the working fluid. A higher cycle thermal efficiency can be achieved with a relatively lower turbine inlet temperature, which could enhance the operation's dependability, reduce the system's complexity and save on costs. Furthermore, the lower turbine inlet temperature of the s-CO_2 Brayton cycle makes the applications possible in solar energy and geothermal power generation, waste heat recovery, and nuclear power generation [2–6]. Moreover, because it is an environmentally friendly working fluid, no pollution is generated in the power generation process of the s-CO_2 Brayton cycle. However, more challenges bring to the key power generation component, i.e., the s-CO_2 radial inflow turbine design, resulting from unique thermal-physical properties. The geometry scaling effect is a salient issue that needs to be resolved due to the smaller geometry of the s-CO_2 turbine [7]. Hence, the radial inflow design with high efficiency is a fundamental issue for applying the advanced s-CO_2 Brayton cycle.

Sandia National Laboratory [8] performed the pioneering experimental work to test the s-CO_2 Brayton cycle and key component performance. In their work, the No. 2 radial

inflow turbine was designed with a power of 213 kW and a total-to-static efficiency of 87%. Bechtel Marine Propulsion Corporation [9] designed the s-CO_2 radial inflow turbine with a total inlet temperature of 299 °C. However, due to several confines in their experimental test, the turbine inlet's total temperature was limited to 232 °C, and the rotating speed could not achieve the nominal value. In the experimental test carried out by the Tokyo Institute of Technology [10], the rotating speed of the s-CO_2 radial inflow was only 55,000 rpm, which was much lower than the design value of 100,000 rpm; this was attributed to the technical limitations of the shaft bearing and sealing. Hence, the output power and the efficiency measured were lower than the designed values. The experimental tests performed by the Korea Institute of Energy Research [11] found the same astriction. The designed rotating speed of their s-CO_2 radial inflow turbine was 70,000 rpm; however, the actual experimental value was limited to 30,000 rpm.

Zhou et al. [12] designed the s-CO_2 radial inflow turbine with the power of 1.5 MW and performed the performance prediction based on the Computational Fluid Dynamics (CFD) method using the software package ANSYS CFX. They found that the predicted total-to-static efficiency is 83.49%, with a deviation less than 5% from the calculated value from their one-dimensional design code. Lv et al. [13] presented an optimization work for the one-dimensional design of the s-CO_2 radial turbine based on the Sequential Quadratic Programming (SQP) optimization algorithm. They revealed the superiority of the optimization work with an improvement of 2.27% on the total-to-static efficiency. Saeed et al. [14] designed s-CO_2 turbines using deep neural networks. Results suggest that the employed multifaceted approach reduces computational time and resources significantly and is required to completely understand the effects of various turbine design parameters on its performance and sizing. Lee et al. [15] developed a code to predict the aerodynamic performance of an s-CO_2 radial inflow turbine under the off-design working condition. The variations were less than 10% between the one-dimensional calculations and the three-dimensional CFD predictions. The energy loss empirical or semi-empirical correlations determine the predicted accuracy. However, limited correlations are available, especially for the s-CO_2 radial inflow turbine. Persky and Sauret [16] evaluated the analytical energy loss correlations used in the preliminary design for the air or gas radial inflow turbine in designing the s-CO_2 turbine. They found that the published loss model configurations may not suit off-design analysis for the s-CO_2 radial inflow turbine. They developed a new loss model configuration with less than a 2% difference in efficiency prediction over the CFD result. With the aid of the CFD method, Keep and Jahn [17] studied the loss contribution for a 300 kW low specific speed s-CO_2 radial inflow turbine. Their results concluded that the end-wall viscous losses in the stator are dominated, which plays a more significant role than that for the gas radial inflow turbine. Yang et al. [18] focused on the leakage loss in the impeller backface cavity for the s-CO_2 radial inflow turbine and revealed the relevance of the leakage loss to the labyrinth seal geometrical parameter.

The present paper provides an optimization design platform based on the one-dimensional design method in Shu et al. [19] to carry forward the efficient s-CO_2 radial inflow turbine design. An in-house code is developed in MATLAB language. The design variables are selected with nozzle velocity coefficient, rotor velocity coefficient, reaction degree, diameter ratio, absolute flow angle rotor inlet, and relative flow angle at the rotor outlet. The optimization function maximizes the total-to-static efficiency with aerodynamic and structural constraints. The build-in function, *fmincon*, is treated as the optimization algorithm. The optimization code is then applied to design the s-CO_2 radial inflow turbine with a power of 2.1 MW. The comparison of the total-to-static efficiency is performed between the CFD simulation and the one-dimensional calculation under the design working condition to validate the current code. The flow field and the performance are also analyzed in detail under the off-design working conditions.

2. One-Dimensional Optimization Design

The general flow chart of the current one-dimensional optimization design for the s-CO_2 radial inflow turbine is shown in Figure 1. The optimization target, the design variables and the relevant lower and upper limits, the initial values of the design variables, and the restricted conditions are required to be specified to run the optimization work. The built-in function in MATLAB, *fmincon*, is selected as the optimization algorithm. Because the *fmincon* function is optimized locally, the predicted optimization result strongly relies on the given starting value. Hence, the final optimization result is obtained by adjusting the initial values and the trial. When the optimization value in the current step is equal to or larger than that in the former step, the optimization process is completed. In the one-dimensional design method for the s-CO_2 radial inflow turbine, the calculated value of the total-to-static efficiency also depends on the thermo-physical properties of the s-CO_2, the selection of the energy loss models, and the specific constrained conditions.

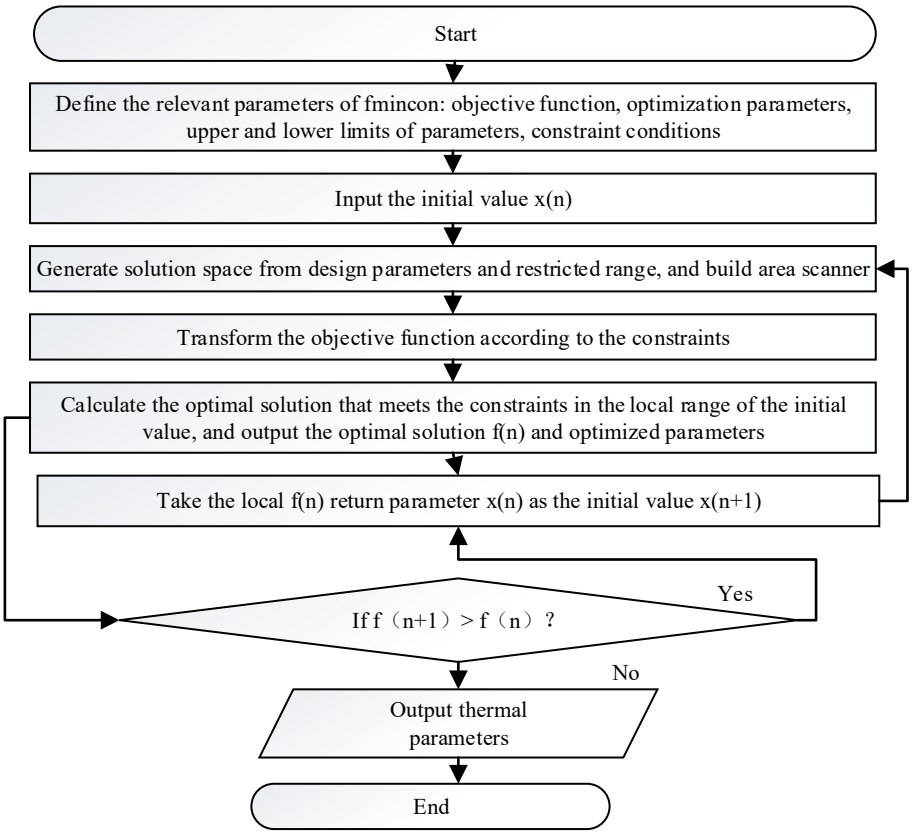


Figure 1. Flow chart of the one-dimensional optimization design.

2.1. Thermo-Physical Property Calculation

Unlike conventional air or gas, working fluid s-CO_2 should be treated as the real working fluid with varying thermo-physical properties. In the current code, the thermo-physical properties are acquired from a featured software package NIST REFPROP [20]. Hence, the thermodynamic parameter at the nozzle inlet, rotor inlet, and rotor exit and the total-to-static efficiency of the s-CO_2 radial inflow turbine can be accurately calculated.

2.2. Optimization Algorithm

The optimization algorithm is the fundamental part of an optimization issue, determining the local or global way and the optimization time. The optimization function, *fmincon*, is commonly applied in constrained nonlinear multivariable nonlinear system optimization problems [21]. The option SQP is chosen for the algorithm option. The Hessian matrix is updated using the BFGS algorithm in the quadratic programming problem. Its major

advantages include succinct code, simple usage, and fewer iterations. The comparison test for the current one-dimensional optimization design showed that the iteration steps are 36, much lower than the iteration step of 120 for the Simulated Annealing Approach. The confinement factor is that only the local optimum result can be acquired, which may differ from the optimum global result. In the present study, the initialized variables are carefully given using the screening method [22] for the radial inflow turbine design. Furthermore, the additional iterative process shown in Figure 1 is applied to pursue the global optimum solution.

2.3. One-Dimensional Design Method

The total-to-static efficiency η_s can be calculated by considering several energy losses, which is given by:

$$\eta_s = [(\eta_u - \zeta_f)\eta_\Delta - \zeta_i]\eta_e \quad (1)$$

where η_u is the peripheral efficiency, ζ_f is the disk friction energy loss coefficient, η_Δ is the clearance efficiency, ζ_i is the incidence loss coefficient, η_e is the partial admission efficiency.

From the energy standpoint, the peripheral efficiency η_u is calculated by:

$$\eta_u = 1 - \zeta_n - \zeta_r - \zeta_{c2} \quad (2)$$

where ζ_n, ζ_r, and ζ_{c2} are the energy loss coefficients in the nozzle, rotor blade, and the leaving velocity at rotor exit.

The peripheral efficiency η_u can also be expressed by the design variables as follow:

$$\eta_u = 2x_a\left(\varphi\cos\alpha_1\sqrt{1-\Omega} - \overline{D}_2^2 x_a + \overline{D}_2\psi\cos\beta_2\sqrt{\Omega + \varphi^2(1-\Omega) + \overline{D}_2^2 x_a^2 - 2x_a\varphi\cos\alpha_1\sqrt{1-\Omega}}\right) \quad (3)$$

where x_a is the velocity ratio, φ and ψ are the nozzle velocity coefficient and rotor blade velocity ratio, α_1 is the absolute flow angle at rotor inlet, β_2 is the relative flow angle at rotor exit, Ω is the reaction degree, $\overline{D}_2$ is wheel diameter ratio. The definitions of x_a, φ, ψ, and $\overline{D}_2$ can be referred to in [19].

The disk friction loss coefficient ζ_f is given by:

$$\zeta_f = \frac{1000}{G\Delta h_s}\cdot\frac{f\rho_1 D_1^2}{1.36}\cdot\left(\frac{u_1}{100}\right)^3 \quad (4)$$

where G is the mass flow rate, Δh_s is the turbine isentropic enthalpy drop, f is the coefficient with a constant value of 4, ρ_1, D_1, and u_1 are the density, diameter, and peripheral velocity at the rotor inlet.

The expression of clearance efficiency η_Δ is as follows:

$$\eta_\Delta = 1 - 1.3(\Delta r / l_m) \quad (5)$$

where Δr is the radial clearance between the shroud and the casing, l_m is the arithmetic mean blade height.

The current radial inflow design assumes the full admission pattern and the partial admission efficiency η_e equals 1.

The incidence loss ζ_i is additionally considered in the current study, which is given by:

$$\zeta_i = \frac{{w_1}^2\sin^2 i_1}{2\Delta h_s} \quad (6)$$

where w_1 is the relative velocity and relative flow angle at the rotor inlet, i_1 is the incidence angle at the rotor inlet. The definition of i_1 is as follows:

$$i_1 = \beta_{1b} - \beta_1 \quad (7)$$

where β_{1b} is the rotor inlet blade angle of 90°, β_1 is the relative flow angle at the rotor inlet.

2.4. Design Constraints and Optimization Function

As seen in the one-dimensional design method, seven design parameters influence the final total-to-static efficiency of the radial inflow turbine. The upper and lower limits of each design parameter for the current design are listed in Table 1, following the suggested values in [19]. Note that the design parameters vary within a wide region, providing sufficient wide design space for the following optimization.

Table 1. Design variable and the relevant value region.

Design Variable	Value Region
Velocity ratio x_a	0.63~0.72
Reaction degree Ω	0.36~0.5
Nozzle velocity coefficient φ	0.92~0.97
Rotor inlet absolute flow angle α_1 (°)	14~25
Rotor exit relative flow angle β_2 (°)	20~45
Wheel diameter ratio $\overline{D}_2$	0.35~0.55
Rotor blade velocity coefficient ψ	0.75~0.90

The aerodynamic limitations and structural constraints must be considered for the one-dimensional optimization design. In the current study, the followings constraints are covered and listed in Table 2. The incidence angle limitation avoids severe reverse flow and the excessive incidence loss at the rotor inlet. The point of the Mach number constraint is to prevent the energy loss and the secondary flow loss from the shock wave. The absolute flow angle at the rotor exit is bounded from 85° to 95°, which guarantees the close axial flow direction for the working fluid at the rotor exit to avoid excessive leaving velocity energy loss. The meridional passage geometry depends on the specific values of the relative shroud diameter and the hub diameter. Hence, the current constraints are assumed to avoid excessive expansion in the meridional passage. When the relative blade height is smaller than its lower limit, the blade height may be too small, especially for the s-CO_2 radial inflow turbine with a heavy working fluid. However, the relative blade height with a large value would influence the shape of the meridional passage.

Table 2. Constraint conditions.

Constrained Variable	Value
Incidence angle at rotor inlet i_1 (°)	−20~+10
Mach number at rotor inlet	≤1.4
Absolute flow angle at rotor exit (°)	85~95
Relative shroud diameter at rotor exit	≤0.85
Relative hub diameter at rotor exit	≥0.12
Relative blade height at rotor inlet	0.02~0.17

Under the consideration of the constraints mentioned above, the optimization function is given as follows:

$$fmincon(1/\eta_s) = f\left(x_a, \Omega, \alpha_1, \beta_2, \varphi, \psi, \overline{D}_2\right) \quad (8)$$

The *fmincon* function is to find the minimum. When the minimum of $1/\eta_s$ is achieved, the maximum of η_s is obtained equivalently. Hence, the reciprocal of η_s is supposed to be the optimization function.

2.5. Optimization Result

A design case is performed to validate the current in-house one-dimensional optimization design code. The design specifications of the s-CO_2 radial inflow turbine are listed in Table 3.

Table 3. Design specifications.

Parameter	Specification
Mass flow rate (kg/s)	16.0
Rotating speed (r/min)	42,000
Inlet total pressure (MPa)	24.6
Inlet total temperature (K)	823
Outlet static pressure (MPa)	8.5
Output power (MW)	2.1

In the optimization process, the numbers of nozzle and rotor blades are fixed as constant values of 33 and 19, respectively. The one-dimensional design results originated from the initial design parameters, and the optimization results are listed in Table 4. It is seen that the optimal set of the seven design variables results in a large rotor geometry and a slightly higher specific speed than the initial design. The optimal design provides an output power of 2.118 MW and a total-to-static efficiency of 85.30%.

Table 4. Initial and optimum design results.

Parameter	Initial Value	Optimum Value
Velocity ratio x_a	0.650	0.662
Reaction degree Ω	0.470	0.483
Nozzle velocity coefficient φ	0.95	0.97
Rotor inlet absolute flow angle α_1 (°)	16.0	16.0
Rotor exit relative flow angle β_2 (°)	21.4	25.0
Wheel diameter ratio $\overline{D}_2$	0.430	0.417
Rotor blade velocity coefficient ψ	0.85	0.90
Rotor inlet relative flow angle β_1 (°)	85.55	85.00
Rotor exit absolute flow angle α_2 (°)	78.0	75.0
Nozzle exit diameter (mm)	170.3	170.4
Rotor inlet diameter (mm)	163.8	166.8
Rotor inlet blade height (mm)	3.0	3.3
Rotor exit hub diameter (mm)	43.1	48.6
Rotor exit shroud diameter (mm)	89.8	85.6
Specific speed	13.76	13.84
Output power (MW)	2.056	2.118
Total-to-static efficiency η_s (%)	83.76	85.30

3. Numerical Methodology and Setup

The steady-state, three-dimensional Navier-Stokes equations are solved using the commercial software NUMECA. The turbulence model comparison work for the radial inflow turbine in [23] concluded that the Spalart-Allmaras turbulence model was a suitable choice with good convergence and adaptability. Hence, the Spalart-Allmaras turbulence model is selected for the turbulent closure in the current study.

The three-dimensional model is generated based on the one-dimensional optimization design geometry, as shown in Figure 2. In the current simulation, one nozzle passage and the rotor blade passage are selected as the computational domain to save the computational cost. The structured meshes are generated using IGG-AutoGrid5, shown in Figure 3. The O4H and HI topology structures are applied for the mesh generation in the nozzle passage and the rotor blade passage. The meshes around the endwall, nozzle, and rotor blade surfaces are refined with an expansion ratio of 1.2 to describe the velocity boundary layers. The computational meshes stratify the numerical simulation standards with an orthogonality angle of less than 20°, an aspect ratio of less than 2500, and an extension ratio of less than 2.

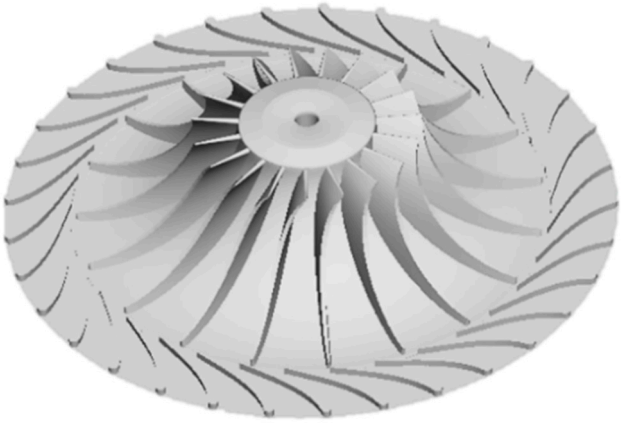


Figure 2. Overview of the designed radial inflow turbine.

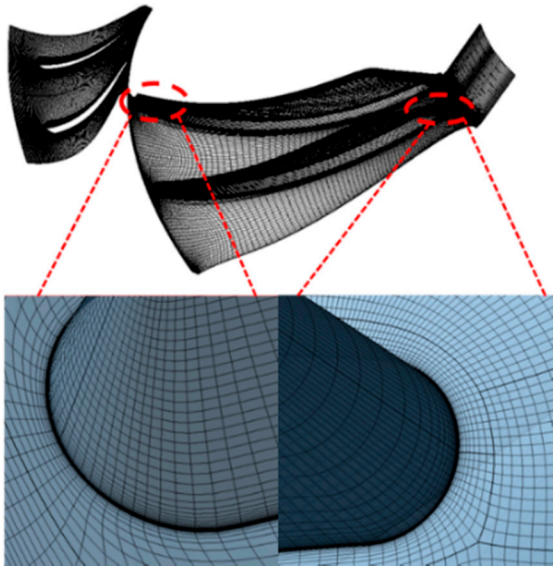


Figure 3. Computational mesh.

A grid independence test is performed to verify the accuracy of the numerical results. Figure 4 shows the total-to-static efficiency variation at five computation mesh resolutions. It is observed that the value of total-to-static efficiency is nearly unchanged since the mesh resolution is higher than 1.72 million. Hence, the mesh resolution of 1.72 million is adopted for the following simulations to balance the prediction accuracy and computation time. The mesh resolutions for the nozzle passage and rotor blade passages are 0.89 million and 0.83 million, respectively.

Alireza et al. [24] pointed out that the thermal-physical properties of the s-CO_2 significantly impact the prediction accuracy for the performance and flow field of the radial inflow turbine. Hence, the real gas thermal-physical properties are generated using a built-in code, TabGen, in the software NUMECA. Because the table generation technique is adopted in the code TabGen, table resolution must be determined in advance. Based on the design specifications for the radial inflow turbine listed in Table 3, the pressure ranges from 5 MPa to 30 MPa, and the temperature ranges from 400 K to 1000 K for the table generation. Note that the thermal-physical properties follow the perfect gas law with explicit functions, which change successively depending on the temperature and pressure at a specific thermodynamic state of CO_2. It is seen in Table 5 that the perfect gas thermal-physical properties lead to a deviation of nearly 3% less in the total-to-static efficiency than the real gas ones. Combatively, only a deviation of 0.01% occurs among

different table resolutions. Therefore, the table resolution of 201 × 201 is adopted in the following simulations.

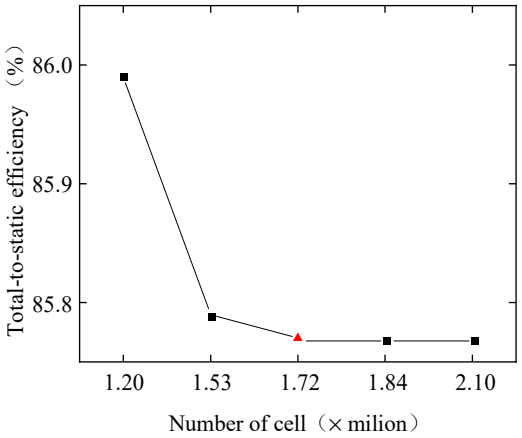


Figure 4. Mesh independence study.

Table 5. Table resolution test of the thermal-physical properties.

Gas Type	Resolution	Total-to-Static Efficiency
Perfect gas	/	82.82%
Real gas	101 × 101	85.78%
	201 × 201	85.77%
	301 × 301	85.77%

However, the thermal-physical properties with a high resolution degrade the computation stability; hence, a low value of the CFL number is required to improve the stability. The CFL number is set as 0.5 in the trade-off between the computation time and stability for the current simulations.

The boundary conditions in simulations are set up as follows. The total pressure and temperature are imposed at the nozzle inlet, and static pressure is set at the rotor exit. The domain of the nozzle passage is stationary, and the domain of the rotor blade passage is rotational. The boundary conditions can be seen in Table 3 for the simulation of the design working conditions. For the simulations under off-design working conditions, the static pressure at the rotor exit varies to achieve the given total-to-static expansion ratio, and the rotational speed differs. The wall surfaces at the hub, blade, and shroud are assumed to be adiabatic, smooth, and in no-slip condition. When the root means square residuals of all variables are lower than 10–6, and the variation of mass flow rate entering into the nozzle passage is less than 0.5%, the convergence of the CFD simulation is achieved.

4. Numerical Result Analysis and Discussion

4.1. Design Working Condition

The comparison between the predicted performance obtained from the three-dimensional simulation and the designed data is listed in Table 6. It is seen that the prediction of mass flow rate, output power, and total-to-static pressure agree well with the designed data in the one-dimensional optimization design. The predictions are slightly higher than the designed data, with a maximum difference of 1.33% for the mass flow rate. The deviation of the total-to-static efficiency is only 0.47%.

Figure 5 represents the streamlines in the nozzle and rotor blade passages. It is observed that the velocity varies gradually along the flow passage, and the streamlines distribute uniformly. There is no obvious swirl flow and separation, which demonstrates a good flow property for the current radial inflow turbine at the design working condition.

Table 6. Evolution of the one-dimensional design.

Parameter	Design	Prediction	Error (%)
Total-to-static expansion ratio	2.896	2.896	0.00
Mass flow rate (kg/s)	16	16.213	1.33
Output power (MW)	2.118	2.135	0.80
Total-to-static efficiency (%)	85.30	85.77	0.47

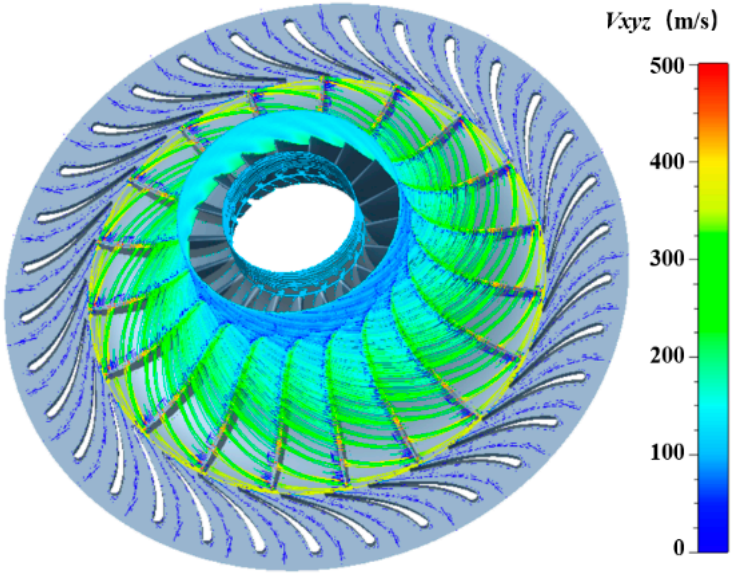


Figure 5. Streamlines in the nozzle and rotor passages.

As presented in Figure 6, the Mach number at 50% blade span gradually increases along the nozzle passage, and the maximum value of 1.26 occurs at the nozzle exit. Although the transonic flow exists in the nozzle passage, the maximum is still within the limits of the Mach number in Table 2.

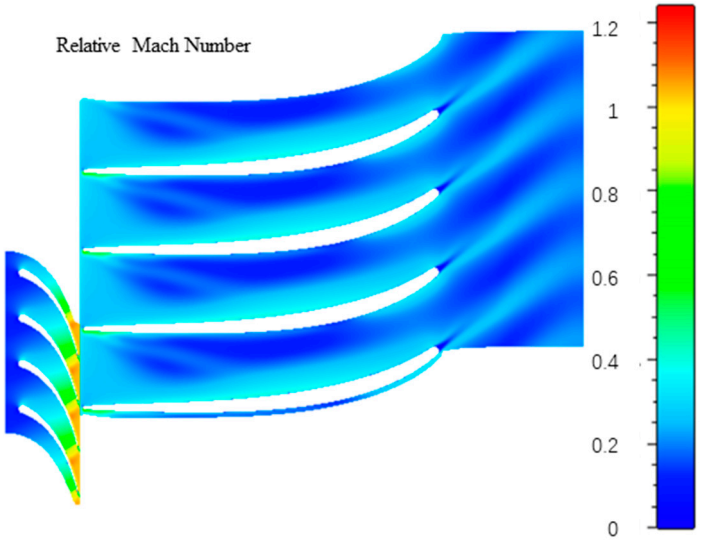


Figure 6. The contour of relative Mach number at 50% blade span.

The static pressure and temperature distribution at 50% blade span are shown in Figure 7. The static pressure and temperature drop gradually inside the turbine. The distributions of the static pressured drop and the temperature drop are reasonable with no abrupt changes.

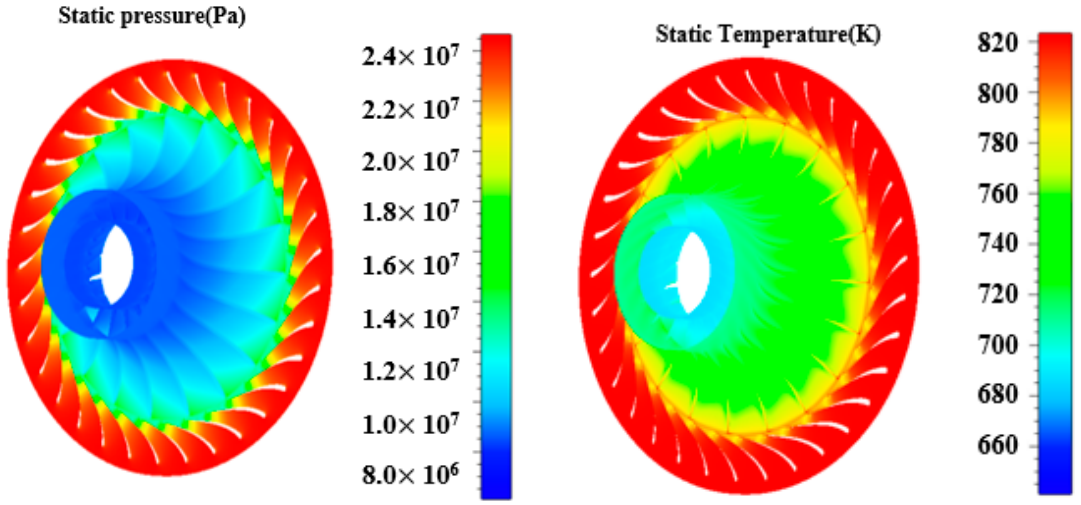


Figure 7. Contours of static pressure and temperature at 50% blade span. (**a**) Static pressure; (**b**) static temperature.

The variations of the enthalpy and entropy in the radial inflow turbine are represented in Figure 8. It is seen that the enthalpy drops uniformly along the flow passage in Figure 8a. As shown in Figure 8b, the entropy reduction changes smoothly along most flow passages. The entropy varies from 2.667 to 2.856 kJ/(kg·K). There is an abrupt increase of about 0.1 kJ/(kg·K) at the interface between the stationary and rotational domains due to the irreversible shock wave energy at the nozzle exit.

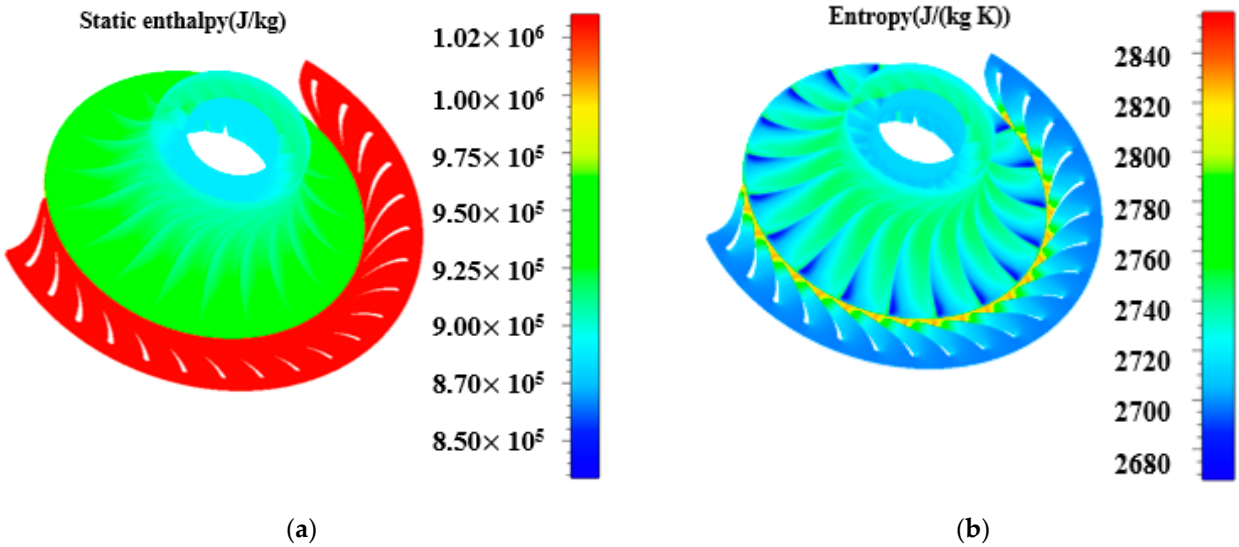


Figure 8. Contours of enthalpy and entropy at 50% blade span. (**a**) Static enthalpy; (**b**) entropy.

4.2. Off-Design Working Conditions

The performance curves of the mass flow rate to the expansion ratio at 70–110% nominal rotational speeds are presented in Figure 9. The benchmark value is set as the nominal rotational speed of 42,000 r/min. As seen in Figure 9, the mass flow rate increases first at the nominal rotational speed and then chokes with the expansion ratio. The mass flow rate approaches the choked mass flow rate when the expansion ratio is 2.896 at the design working condition. At the off-design working conditions, the rotational speed significantly impacts the mass flow rate when the expansion ratio is lower than 3.0. The mass flow rate increases at the same expansion ratio as the rotational speed increases. However, if the

expansion ratio is higher than 3.0, the rotational speed variation has little impact on the mass flow rate. The radial inflow turbine is always choked with an expansion ratio higher than 3.788 regardless of the rotational speed. The maximum allowable expansion ratio is 5.47, and the corresponding choked mass flow rate is 16.358 kg/s.

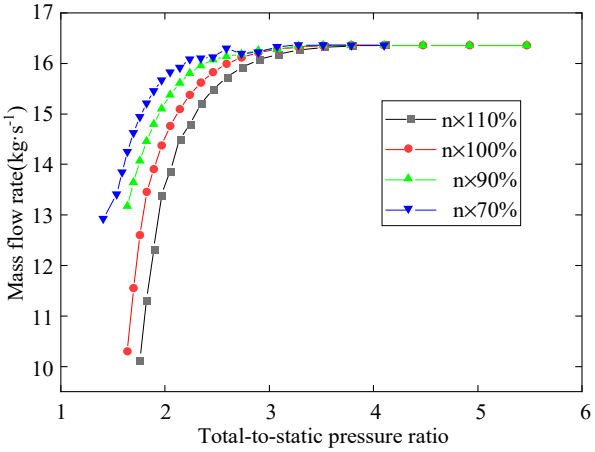


Figure 9. Performance curves of mass flow rate to expansion ratio at 70–110% nominal rotational speeds.

Figure 10 shows the variation curves of the total-to-static efficiency to the expansion ratio at different rotational speeds. At the nominal rotational speed, the value of the total-to-static efficiency increases and decreases with the expansion ratio. The total-to-static efficiency at the design working condition is 85.77%, close to the maximum value at the performance curve. This means that the current one-dimensional optimization design is appropriate. Moreover, the total-to-static efficiency always yields a value higher than 70%, with the expansion ratio region of 1.76–5.47. The performance curve and the local maximum total-to-static efficiency point shift towards the left with the decrease in rotational speed. The total-to-static efficiencies are higher than 75%, with an expansion ratio of 1.75–4.48 at 80–110% nominal rotational speed. However, the total-to-static efficiency is lower than 70%, with most expansion ratios at the 70% nominal rotational speed. Hence, it is suggested that the current radial inflow turbine avoid operating under these working conditions.

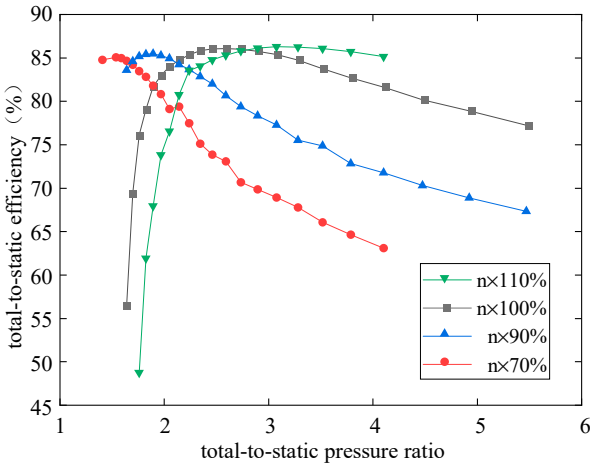


Figure 10. Performance curves of total-to-static efficiency to expansion ratio at 70–110% nominal rotational speeds.

5. Conclusions

In this paper, the one-dimensional optimization design code is developed for the s-CO_2 radial inflow turbine. The key optimization function is the built-in function *fmincon*

in MATLAB. A case study is performed using the developed code for the radial inflow turbine design with an output power of 2.1 MW. The predicted performance and detailed flow field are obtained from the simulation results for the three-dimensional model using the software package NUMECA. Several major conclusions are reached as follows:

(1) The developed one-dimensional optimization design method is validated by comparing the initial and optimum designs. The total-to-static efficiency for the optimum design is 85.30%, with an absolute improvement of 1.54%.
(2) The performance deviations between the three-dimensional prediction result and the one-dimensional design data are lower than 2%. Under the design working condition, the total-to-static efficiency is close to the maximum value at the nominal rotational speed. The static pressure, temperature, enthalpy, and entropy distribute uniformly in the nozzle and rotor blade flow passages, demonstrating good performance for the current radial inflow turbine under the designed working conditions.
(3) The performance analysis revealed that the total-to-static efficiency is higher than 75% at 80–110% nominal rotational speed.

Author Contributions: Conceptualization, formal analysis, and funding acquisition, Z.T.; validation and writing—original draft preparation, Z.S.; writing—review and editing, and supervision, C.Z.; formal analysis and visualization, H.X.; methodology, Y.S. All authors have read and agreed to the published version of the manuscript.

Funding: This research was funded by the National Natural Science Foundation of China, grant number 51976139.

Institutional Review Board Statement: Not applicable.

Informed Consent Statement: Not applicable.

Data Availability Statement: Not applicable.

Conflicts of Interest: The authors declare no conflict of interest.

References

1. Dostal, V. A Supercritical Carbon Dioxide Cycle for Next-Generation Nuclear Reactors. Ph.D. Thesis, Massachusetts Institute of Technology, Cambridge, UK, 2004.
2. Iverson, B.D.; Conboy, T.M.; Pasch, J.J.; Kruizenga, A.M. Supercritical CO_2 Brayton cycles for solar-thermal energy. *Appl. Energy* **2013**, *111*, 957–970. [CrossRef]
3. Sun, L.; Wang, Y.; Wang, D.; Xie, Y. Parametrized analysis and multi-objective optimization of supercritical CO_2 (s-CO_2) power cycles coupled with parabolic trough collectors. *Appl. Sci.* **2020**, *10*, 3123. [CrossRef]
4. Ruiz-Casanova, E.; Rubio-Maya, C.; Pacheco-Ibarra, J.J.; Ambriz-Díaz, V.M.; Romero, C.E.; Wang, X. Thermodynamic analysis and optimization of supercritical carbon dioxide Brayton cycles for use with low-grade geothermal heat sources. *Energy Convers. Manag.* **2022**, *216*, 112978. [CrossRef]
5. Liang, Y.; Bian, X.; Qian, W.; Pan, M.; Ban, Z.; Yu, Z. Theoretical analysis of a regenerative supercritical carbon dioxide Brayton cycle/organic Rankine cycle dual loop for waste heat recovery of a diesel/natural gas dual-fuel engine. *Energy Convers. Manag.* **2019**, *197*, 111845. [CrossRef]
6. Wu, P.; Ma, Y.; Gao, C.; Liu, W.; Shan, J.; Huang, Y.; Wang, J.; Zhang, D.; Ran, X. A review of research and development of supercritical carbon dioxide Brayton cycle technology in nuclear engineering applications. *Nucl. Eng. Des.* **2019**, *368*, 110767. [CrossRef]
7. Sashadri, L.; Raja, H.N.; Kumar, P.; Nassar, A.; Giri, G.; Moroz, L. Supercritical carbon dioxide turbomachinery options for kilowatt to gigawatt level power generation. In Proceedings of the ASME 2019 Gas Turbine India Conference, Tamil Nadu, India, 5–6 December 2020. Volume 2: Combustion, Fuels, and Emissions; Renewable Energy: Solar and Wind; Inlets and Exhausts; Emerging Technologies: Hybrid Electric Propulsion and Alternate Power Generation; GT Operation and Maintenance; Materials and Manufacturing (Including Coatings, Composites, CMCs, Additive Manufacturing), Analytics and Digital Solutions for Gas Turbines/Rotating Machinery.
8. Pasch, J.; Conboy, T.; Fleming, D.; Rochau, G. *Supercritical CO_2 Recompression Brayton Cycle: Completed Assembly Description*; Report: SAND2012-9546; Sandia National Laboratories: Albuquerque, NM, USA; Livermore, CA, USA, 2012.

9. Pasch, J.; Conboy, T.; Fleming, D.; Carlson, M.; Rochau, G. Steady state supercritical carbon dioxide recompression closed Brayton cycle operating point comparison with predictions. In Proceedings of the ASME Turbo Expo 2014: Turbine Technical Conference and Exposition, Düsseldorf, Germany, 16–20 June 2014. Volume 3B: Oil and Gas Applications; Organic Rankine Cycle Power Systems; Supercritical CO_2 Power Cycles, Wind Energy.
10. Utamura, M.; Hasuike, H.; Yamamoto, T. Demonstration test plant of closed cycle gas turbine with supercritical CO_2 as working fluid. *Strojarstvo* **2010**, *52*, 459–465.
11. Cho, J.; Choi, M.; Baik, Y.J.; Lee, G.; Ra, H.S.; Kim, B.; Kim, M. Development of the turbomachinery for the supercritical carbon dioxide power cycle. *Int. J. Energy Res.* **2016**, *40*, 587–599. [CrossRef]
12. Saeed, M.; Berrouk, A.S.; Burhani, B.M.; Alatyar, A.M.; Wahedi, Y.F.A. Turbine design and optimization for a supercritical CO_2 cycle using a multifaceted approach based on deep neural network. *Energies* **2021**, *14*, 7807. [CrossRef]
13. Zhou, A.; Song, J.; Li, X.; Ren, X.; Gu, C. Aerodynamic design and numerical analysis of a radial inflow turbine for the supercritical carbon dioxide Brayton cycle. *Appl. Therm. Eng.* **2018**, *132*, 245–255. [CrossRef]
14. Lv, G.; Yang, J.; Shao, W.; Wang, X. Aerodynamic design optimization of radial-inflow turbine in supercritical CO_2 cycles using a one-dimensional model. *Energy Convers. Manag.* **2018**, *165*, 827–839. [CrossRef]
15. Lee, S.; Yaganegi, G.; Mee, D.J.; Guan, Z.; Gurgenci, H. Part-load performance prediction model for supercritical CO_2 radial inflow turbines. *Energy Convers. Manag.* **2021**, *235*, 113964. [CrossRef]
16. Persky, R.; Sauret, E. Loss models for on and off-design performance of radial inflow turbomachinery. *Appl. Ther. Eng.* **2019**, *150*, 1066–1077. [CrossRef]
17. Keep, J.A.; Jahn, I.H.J. Numerical loss investigation of a small scale, low specific speed supercritical CO_2 radial inflow turbine. *J. Eng. Gas Turbines Power* **2019**, *141*, 091003. [CrossRef]
18. Yang, J.; Zhao, F.; Zhang, M.; Liu, Y.; Wang, X. Numerical analysis of labyrinth seal performance for the impeller backface cavity of a supercritical CO_2 radial inflow turbine. *Comput. Model. Eng. Sci.* **2021**, *126*, 935–953. [CrossRef]
19. Shu, S.Z.; Zhu, L.; Ke, X.L.; Jiang, Z.K. *Principle of Turbomachinery*, 3rd ed.; Tsinghua University Press: Beijing, China, 1991; pp. 150–172.
20. Lemmon, E.W.; Mclinden, M.O.; Huber, M.L. *NIST Standard Reference Database 23, Version 10.0, Reference Fluid Thermodynamic and Transport Properties-REFPROP*; National Institute of Standards and Technology (NIST): Boulder, CO, USA, 2018.
21. Chen, Y.; Cheng, Z.; Huang, Z. Optimal design of lifting mechanism of linkage hydraulic lifting dam based on matlab. *J. Phys. Conf. Ser.* **2021**, *1948*, 012128. [CrossRef]
22. Li, Y.S.; Lu, G. *Radial Inflow Turbine and Centrifugal Compressor*, 1st ed.; China Machine Press: Beijing, China, 1987; pp. 34–80.
23. Ameli, A.; Uusitalo, A.; Turunen-Saaresti, T.; Backman, J. Numerical sensitivity analysis for supercritical CO_2 radial turbine performance and flow field. *Energy Procedia* **2017**, *129*, 1117–1124. [CrossRef]
24. Lou, L.; Du, W.; Wang, S.T. Effect of turbulence model on the performance of a SCO_2 radial turbine. *Heat Transf. Res.* **2020**, *51*, 173–192.